

Dreaming of Electrical Waves: Generative Modeling of Cardiac Excitation Waves using Diffusion Models

Tanish Baranwal,^{1,2} Jan Lebert,¹ and Jan Christoph^{1,*}

¹*Cardiovascular Research Institute, University of California, San Francisco, USA*

²*Department of Electrical Engineering and Computer Science, University of California, Berkeley, USA*

(Dated: December 25, 2023)

Electrical waves in the heart form rotating spiral or scroll waves during life-threatening arrhythmias such as atrial or ventricular fibrillation. The wave dynamics are typically modeled using coupled partial differential equations, which describe reaction-diffusion dynamics in excitable media. More recently, data-driven generative modeling has emerged as an alternative to generate spatio-temporal patterns in physical and biological systems. Here, we explore denoising diffusion probabilistic models for the generative modeling of electrical wave patterns in cardiac tissue. We trained diffusion models with simulated electrical wave patterns to be able to generate such wave patterns in unconditional and conditional generation tasks. For instance, we explored inpainting tasks, such as reconstructing three-dimensional wave dynamics from superficial two-dimensional measurements, and evolving and generating parameter-specific dynamics. We characterized and compared the diffusion-generated solutions to solutions obtained with biophysical models and found that diffusion models learn to replicate spiral and scroll waves dynamics so well that they could serve as an alternative data-driven approach for the modeling of excitation waves in cardiac tissue. For instance, we found that it is possible to initiate ventricular fibrillation (VF) dynamics instantaneously without having to apply pacing protocols in order to induce wavebreak. The VF dynamics can be created in arbitrary ventricular geometries and can be evolved over time. However, we also found that diffusion models ‘hallucinate’ wave patterns when given insufficient constraints. Regardless of these limitations, diffusion models are an interesting and powerful tool with many potential applications in cardiac arrhythmia research and diagnostics.

I. INTRODUCTION

Waves in excitable media exhibit complex spatio-temporal dynamics [1, 2]. In two-dimensional media, they form linear, focal or rotating spiral-shaped waves or compositions thereof. In three-dimensional media, they manifest as planar or spherical focal waves, or take on more complicated rotational shapes referred to as scroll waves. Spiral and scroll wave dynamics have been studied for many decades, as they are associated with heart rhythm disorders, such as atrial fibrillation, polymorphic ventricular tachycardia, or ventricular fibrillation [2–12]. In the heart, electrical excitation initiates the contraction of the heart muscle and it is hypothesized that the abnormal, rapid and irregular contractions during tachyarrhythmias are caused by spiral- and scroll-shaped waves of electrical excitation.

The electrical waves can be reproduced and studied in computer simulations using biophysical models [13–15]. These models consist of coupled partial differential equations (PDEs), which describe the electrical excitability u and refractoriness r of cardiac muscle cells and the coupling between them, see eqs. (1–2). The equations model reaction-diffusion dynamics, where the exchange of currents through ion channels between cells are modeled as a diffusive process and the cells as nonlinear oscillators. Integrating these equations in time and over space in a

spatially extended system using, for instance, the finite difference or finite element method produces nonlinear waves of electrical excitation mediated via diffusion.

Diffusion, on the other hand, is a term that has recently emerged in the field of artificial intelligence (AI), referring to a class of generative neural networks which employ a diffusive process to generate data [16–18]. During the training procedure, noise is iteratively added to the training data and the neural networks, termed denoising diffusion probabilistic models (DDPMs) [18] or diffusion models, learn to reverse this process, ultimately enabling them to create data from noise, see Fig. 1. Diffusion models are very successful in generating data such as images [19–21], videos [22], and audio [23], and they are increasingly also used for technical applications in physics, engineering, medicine, and biology [24–27]. Diffusion models likely also have many useful applications in cardiology that yet have to be explored. For example, they could be used in electrophysiological studies to generate synthetic action potential wave patterns and arrhythmia morphologies, either to fill in or reconstruct missing measurement data, or to simulate cardiac dynamics in a data-driven fashion. Diffusion-generated solutions could be particularly useful in situations in which measurements can only be obtained partially or indirectly, or when biophysical model equations or parameters are lacking.

Here, we explore diffusion models for their application in cardiac electrophysiology and arrhythmia research. In this numerical study, we investigated whether diffusion models can be used to reconstruct or simulate electrical impulse phenomena, such as spiral and scroll waves,

* <https://cardiacvision.ucsf.edu>; jan.christoph@ucsf.edu

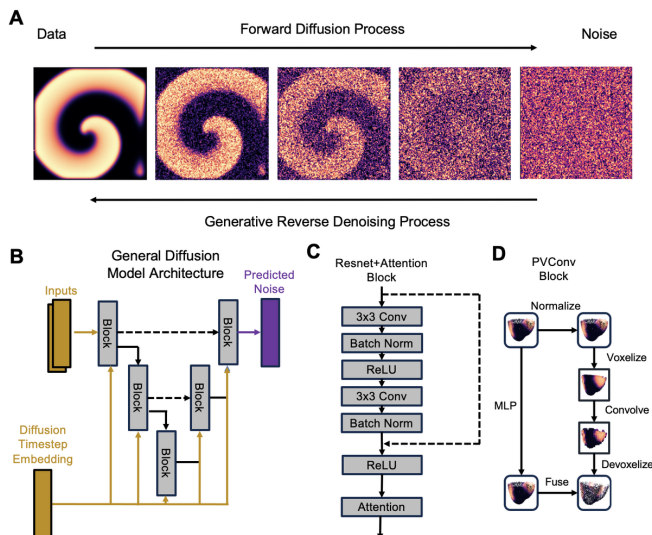


FIG. 1. Diffusion-based generative modeling of electrical wave dynamics in cardiac tissue. **A** Forward diffusion process and generative reverse denoising process. The training data consists of spiral and scroll wave dynamics in excitable media. **B** General diffusion model architecture for processing image data with underlying U-Net architecture. **C** ResNet Attention block. **D** Diffusion model for generating scroll waves in heart-shaped geometries represented as pointclouds with corresponding scalar-valued data (Point-Voxel Diffusion [28]).

in computer simulations of excitable media. We simulated electrical spiral and scroll waves in two- and three-dimensional square-, bulk- and heart-shaped tissues with isotropic and anisotropic diffusive spread of the excitation, and trained different diffusion models to i) in-paint spiral wave dynamics, see section III B, ii) reconstruct three-dimensional scroll wave dynamics from two-dimensional observations, see section III A, iii) generate parameter-specific wave dynamics, see section III G, and iv) predict the evolution of wave dynamics over time in analogy to integrating the dynamics, see section III E. We determined how reliable diffusion models are when generating such spatio-temporal physiological dynamics. Generative neural networks, such as diffusion models, generative adversarial networks (GANs), or large language models (LLMs) are known to be capable of producing a continuum of output including false or undesired output, which is often referred to as ‘hallucination’. We show that diffusion models can generate electrical waves in many different ways: out of the blue in an unconstrained generative process or when the generative process is guided or constrained by parameters or boundary conditions such as partial data, or a recent dynamical state of the system. In particular, the latter generative mode corresponds to diffusion-based data-driven modeling of cardiac dynamics. We found that hallucination occurs when the generation task is insufficiently constrained, which raises concerns over the reliability of diffusion models in diagnostic applications.

II. METHODS

A. Simulations of Electrical Wave Dynamics in Heart Muscle Tissue

We simulated nonlinear waves of electrical excitation in i) two-dimensional rectangular-shaped, ii) three-dimensional bulk-shaped, and iii) three-dimensional heart-shaped geometries, respectively. In all three cases, we used the phenomenological Aliev-Panfilov model [15] to simulate nonlinear waves of electrical excitation:

$$\frac{\partial u}{\partial t} = \nabla \cdot (\mathbf{D} \nabla u) - ku(u-a)(u-1) - ur \quad (1)$$

$$\frac{\partial r}{\partial t} = \left(\epsilon_0 + \frac{\mu_1 r}{u + \mu_2} \right) (ku(a+1-u) - r) \quad (2)$$

The dynamic variables u and r represent the local electrical excitation and refractoriness in dimensionless, normalized units, respectively. The parameters k , a , ϵ_0 , μ_1 and μ_2 determine the properties of the waves (e.g. excitability, wavelength, conduction speed, number of waves, etc.). We varied the parameters k , and ϵ_0 to change the properties of the excitation waves and produce different training data for different tasks (Task 1-6), see Table I and sections II B 1-II B 6. The simulations in the simplified (rectangular, bulk) and heart-shaped geometries were performed as described in [29] and [31], respectively. Correspondingly, the system of equations (1-2) was integrated using the forward Euler method and the smoothed particle hydrodynamics method [32, 33], respectively. The two-dimensional simulations were isotropic, whereas the three-dimensional simulations were anisotropic with a locally varying fiber direction and faster wave propagation along the fiber direction. The fiber architectures were created as described in [29, 31]. In particular, the bi-ventricular heart geometries and underlying rule-based fiber architectures were randomly initialized as described in [31].

The model parameters were chosen specifically for each task, see Table I. We simulated scroll wave dynamics in a bulk with $128 \times 128 \times 40$ voxels as shown in Fig. 2 using a fixed set of parameters (Task 1). We simulated two different regimes of spiral wave dynamics, as shown in Figs. 4 and 6, using two different parameter sets: one with few (Task 2a, 5a) and one with more spiral waves (Tasks 2b, 5b). We simulated a range of parameter-specific spiral wave dynamics (Task 6), as seen in Fig. 8A,B), by varying the parameters k and ϵ_0 . For each task, we performed hundreds of simulations to generate sufficient training data. For example, for Task 1, we performed 125 simulations, where 100 simulations were used for training and 25 for evaluation, as described in [29]. The initial conditions u_0, r_0 were randomized and therefore different in each simulation, see also [31]. If the spiral or scroll wave dynamics self-terminated prematurely, we restarted the simulation.

Using the simulation data, we generated different training datasets for each task, see Tasks 1-6 in sec-

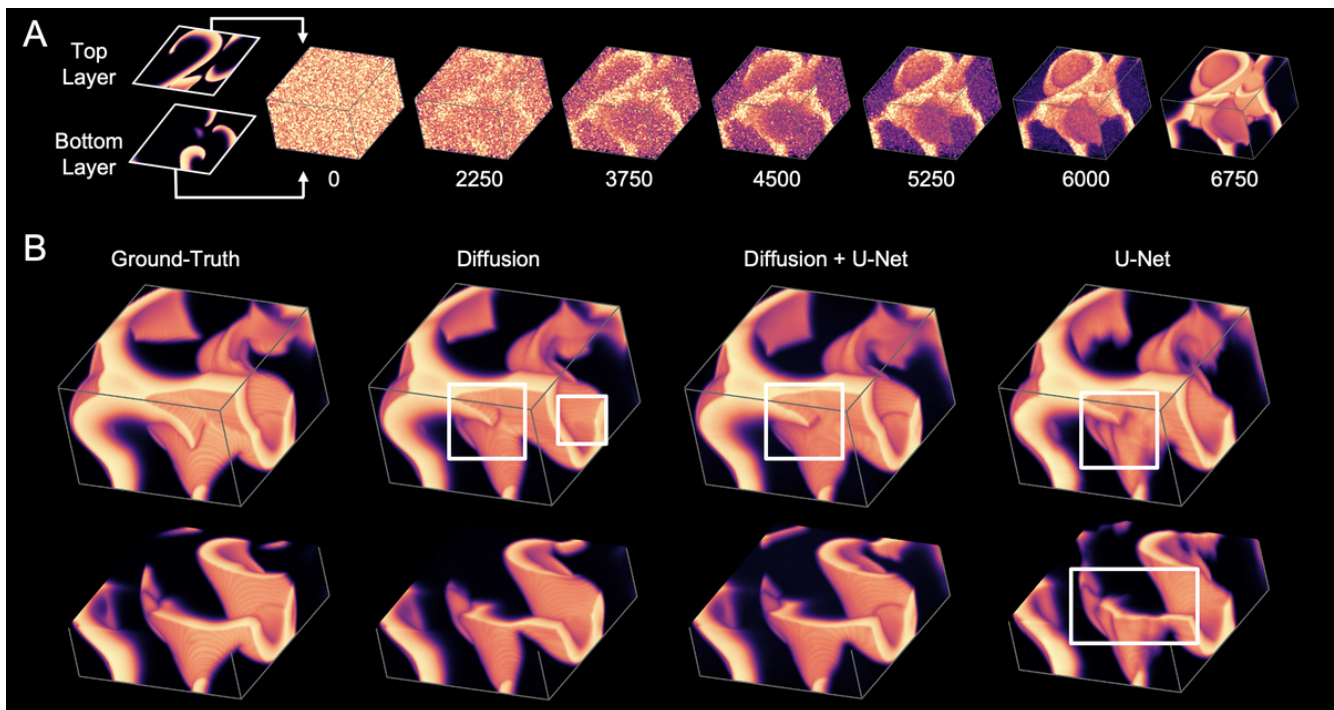


FIG. 2. Diffusion-based reconstruction of scroll wave dynamics inside a three-dimensional bulk from two-dimensional observations of the dynamics on the bulk’s top and bottom surface. The bulk is fully opaque and measurements can only be obtained from its surface. **A** Illustration of diffusion process over denoising iterations. **B** Scroll wave dynamics (left: ground-truth) and reconstructed scroll waves with diffusion (center left), U-Net (right) and U-Net refined with diffusion (center right), see also [29, 30]. While diffusion produces smoother wave patterns than U-Net, particularly at deeper layers, the overall reconstruction accuracies are not significantly different across the three approaches, see also Fig. 3. White squares highlight slight differences between reconstructions and ground-truth. The bulk is $128 \times 128 \times 40$ voxels (aspect ratio was altered to emphasize transmural wave morphology), see also [29]. The simulation parameters are shown in Table I (Task 1).

tion IIB for details. Each training dataset consisted of thousands of samples randomly chosen from the different training simulations. Correspondingly, each evaluation dataset consisted of thousands of samples randomly chosen from the evaluation simulations. Training and evaluation datasets were completely separate datasets.

B. Denoising Diffusion Model

We used a denoising diffusion probabilistic modeling [18] neural network architecture, which we refer to as diffusion model for simplicity. Diffusion models consist of a forward diffusion process and a reverse diffusion process, see Fig. 1. During the forward diffusion process, gaussian noise is added incrementally to an input image until it is indistinguishable from random noise. This produces a sequence of samples (x_0, \dots, x_T) with increasing noise, starting from the data point x_0 from the real data distribution $q(x)$ and ending with what is indistinguishable from an isotropic Gaussian distribution.

$$q(\mathbf{x}_t | \mathbf{x}_{t-1}) = \mathbf{N}(\mathbf{x}_t; \sqrt{1 - \beta_t} \mathbf{x}_{t-1}, \beta_t \mathbf{I}) \quad (3)$$

The step sizes are controlled by a variance schedule β_t .

$$q(\mathbf{x}_{1:T} | \mathbf{x}_0) = \prod_{t=1}^T q(\mathbf{x}_t | \mathbf{x}_{t-1}) \quad (4)$$

When sampling new data from the data distribution $q(x)$, a model p_θ is learned to estimate $q(x_{t-1} | x_t)$, which is also approximated by a gaussian distribution. This is referred to as the reverse diffusion process.

$$p_\theta(x_{0:T}) = p(\mathbf{x}_T) \prod_{t=1}^T p_\theta(\mathbf{x}_{t-1} | \mathbf{x}_t) \quad (5)$$

$$p_\theta(\mathbf{x}_{t-1} | \mathbf{x}_t) = \mathbf{N}(\mathbf{x}_{t-1}; \mu_\theta(\mathbf{x}_t, t), \Sigma_\theta(\mathbf{x}_t, t)) \quad (6)$$

This allows the model p_θ to only have to estimate the two parameters μ and σ of the estimated denoising step. Commonly, σ_θ is fixed to a constant variance schedule and is not learnable. This means that in order to estimate p_θ , a model needs to learn $\mu_\theta(x_t, t)$. Electrical wave dynamics can be treated as image-like data and the U-Net architecture from Dhariwal and Nichol [34] is used to estimate the noise at each step of the reverse diffusion process. The model is trained using pairs taken from the forward diffusion process x_t, x_{t-1} and taking the mean

squared error (MSE) between the noise estimated by the model and the true noise at that step. We implemented different versions of diffusion models for different tasks, as described in the following sections. The conditioned diffusion models for sections IIB 2, IIB 5, and IIB 6 were implemented following Saharia et al. [20] using an implementation by Liangwei Jiang and Yury Belousov [35]. The unconditioned diffusion model for section IIB 3 was implemented following Ho et al. [18] using the Diffusers library [36]. The diffusion model for section IIB 4 was implemented following Zhou et al. [28] using the official codebase. All diffusion models include a U-Net [37] architecture and were implemented in PyTorch [38].

Param.	Task 1	Task 2a/5a	Task 2b/5b	Task 3	Task 4	Task 6
D	D_a	1	1	1	D_a	1
k	8	8.5	7.5	8	8	k'
a	0.05	0.1	0.1	0.05	0.2	0.1
ϵ_0	0.002	0.003	0.001	0.002	0.002	ϵ'_0
μ_1	0.8	0.16	0.16	0.2	0.2	0.16
μ_2	0.3	0.3	0.3	0.3	0.3	0.3

TABLE I. Parameters of biophysical model [15] used to simulate electrical wave patterns. Task 1: Scroll wave dynamics in anisotropic 3D bulk shown in Fig. 2. Tasks 2, 3, 5: Spiral wave dynamics in 2D isotropic medium, see Figs. 4, 6, 7. Task 4: Scroll wave dynamics in (bi-ventricular) heart-shaped medium, see Fig. 5. Task 6: Parameter-specific generation of spiral waves, see Fig. 8. D_a is an anisotropic diffusion tensor, see also [29, 31].

Task 1: Reconstruction of 3D Scroll Wave Dynamics

We trained a diffusion model to predict three-dimensional scroll wave dynamics inside a bulk from two-dimensional observations of the dynamics on the surface of the bulk (Task 1), as described in Lebert et al. [29] and shown in Fig. 2. The model was trained to predict a single three-dimensional snapshot of the excitatory variable $u_t(x, y, z)$ at a given time t at every voxel in a bulk with $128 \times 128 \times 40$ voxels from 5 subsequent two-dimensional snapshots of the dynamics on the bulk’s surface:

$$(u_1(x, y), \dots, u_5(x, y)) \rightarrow \tilde{u}_5(x, y, z) \quad (7)$$

where \tilde{u} is a prediction of the true dynamics u (ground-truth). The snapshots were measured either i) on the top surface only (single-surface mode) resulting in a spatio-temporal measurement consisting of 5 snapshots $(u_1(x, y, 1), \dots, u_5(x, y, 1))$ or ii) on the top and bottom surface (dual-surface mode) resulting in $2 \cdot 5$ snapshots $(u_1(x, y, 1), u_1(x, y, 40), u_2(x, y, 1), \dots, u_5(x, y, 40))$, as described in [29]. The 5 snapshots were sampled at equidistant times $t_1, t_2, t_3, t_4, t_5 = t_{-4\tau}, t_{-3\tau}, t_{-2\tau}, t_{-\tau}, t$ with $u_i = u(t_i)$ over about one rotational period T of the scroll wave dynamics ($\tau = t - t_{-\tau} \approx T/5$), which we

found to provide sufficient information to reconstruct the dynamics, as described in [29, 39, 40]. Accordingly, we conditioned the diffusion model by concatenating these sequences as additional channels in the U-Net inputs (interleaved in dual-surface mode, odd indices for the top layer and even indices for the bottom layer). To explore an alternative extension of our reconstruction approach, we conditioned the diffusion model using the output of a generic U-Net model, which was trained and applied as described in [29], to create a combined model that potentially can take advantage of the strengths of both the U-Net and diffusion models, see also Fig. 3. Accordingly, we conditioned the combined model with the sequences of 5 (or $2 \cdot 5$) two-dimensional snapshots and 1 three-dimensional prediction $\tilde{u}(x, y, z)$ of the U-Net model, which analyzed in turn also 5 snapshots as input. The two- and three-dimensional inputs were concatenated to obtain $(128 \times 128 \times 45)$ or $(128 \times 128 \times 50)$ samples in single- vs. dual-surface mode as conditions, respectively. This leads to a total of 4 conditioning modes that we tested (single- vs. dual-surface, diffusion vs. combination of diffusion + U-Net). Generally, the different model versions required three-dimensional input samples, e.g. $(128 \times 128 \times 5)$ or $(128 \times 128 \times 45)$. To denoise a $128 \times 128 \times 40$ volume image with $5 \cdot 128 \times 128$ snapshots as conditioning, the model corresponds to an $R(128 \times 128 \times 45) \rightarrow R(128 \times 128 \times 40)$ function. However, internally, because the denoising diffusion process works on the intermediate noisy bulk data, the overall data consists of the conditioning data concatenated to the noisy data which then results in an array size of, for example, $128 \times 128 \times 80$. Training was performed with 20,000 training samples, which were generated in 100 simulations, see also section II A, and the model was evaluated on 5,000 separate samples. We used the same simulation data and parameters as in [29], see also Table I.

Task 2: Inpainting of 2D Spiral Wave Dynamics

We trained a diffusion model to inpaint missing data of two-dimensional spiral wave dynamics (Task 2), as shown in Fig. 4. We masked or left out data from a square region at the center of the 128×128 pixel simulation domain and trained the network with corresponding pairs of masked $u_m(x, y)$ and ground-truth data $u(x, y)$ to reconstruct the missing parts of the spiral wave pattern:

$$(u_{m,1}(x, y), \dots, u_{m,5}(x, y)) \rightarrow \tilde{u}_5(x, y) \quad (8)$$

where \tilde{u} is a prediction of the ground-truth dynamics u and the model reads a short spatio-temporal sequence of 5 two-dimensional snapshots as in section IIB 1. Masked pixels were replaced by zeros. We tested how the reconstruction accuracy of the network changes with different mask sizes $m \in [0.05, \dots, 0.8]$ (percentage masked area vs. total area from 5% to 80% in increments of 5%) and with less and more complex wave patterns, see section

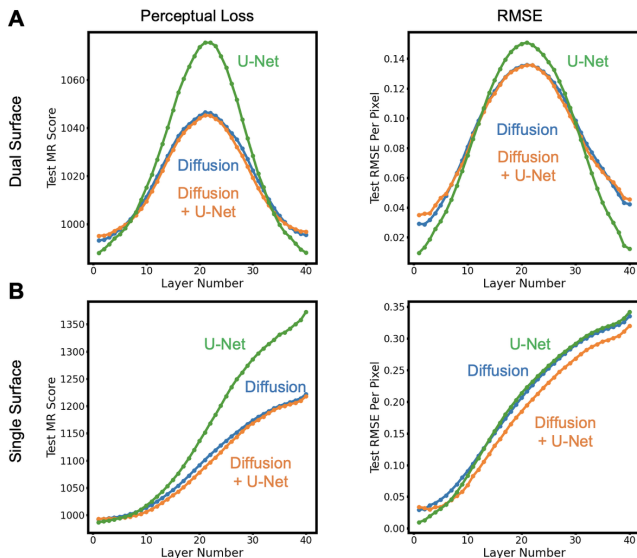


FIG. 3. Transmural reconstruction error per layer number or depth with diffusion (blue), U-Net (green) or diffusion + U-Net (orange), see also Fig. 2. The reconstruction error was quantified using either the perceptual error [41] (left) or absolute difference (RMSE, right). **A** Dual-surface reconstruction analyzing top and bottom layers: U-Net performs worse at midwall, but slightly better closer to the surfaces than diffusion. Perceptual error and RMSE produce very different error profiles. **B** Single-surface prediction: the perceptual error increases more steeply with U-Net as with diffusion, while all models perform similar with RMSE.

III B. We simulated two spiral wave regimes and trained two separate models: i) one with largely only one spiral wave (Task 2a) and ii) one with multiple, more chaotic spiral waves (Task 2b), see Table I for the corresponding simulation parameters. Both models were trained equally with a range of masks with uniform distribution (of the percentage of masked area vs. total area). Training and evaluation was performed with 27, 500 and 6, 000 samples, respectively.

Task 3: Unconditional Generation of Spiral Wave Patterns

We trained a diffusion model to generate two-dimensional spiral wave patterns in an unconditional fashion (Task 3), as also shown in Fig. 7. This means that the model can dream up any spiral wave pattern it can come up with (depending on what data it was trained on) starting from random noise ξ :

$$\xi(x, y) \rightarrow (\tilde{u}, \tilde{r})(x, y) \quad (9)$$

The model is completely unrestricted in that it is not trained to perform certain tasks, such as inpainting, nor conditioned by certain boundary conditions, such as top or bottom layers, or parameters which guide the generative process, as in section II B 6. The model was trained

with 50, 000 training samples generated from spiral wave patterns simulated in an isotropic excitable medium with a fixed parameter set from [42], see also Table I. Each training sample consisted of a single spiral wave pattern defined by its dynamical variables $(u, r)_t(x, y)$ in a 128×128 pixel simulation domain. The training samples were sampled from the last 300 time steps of 1, 000 simulations which ran for a fixed simulation time and were randomly initiated following a random pulse protocol, similarly as used in [42]. After training, the diffusion model outputs a pair of two-dimensional $(\tilde{u}, \tilde{r})_t(x, y)$ -fields or a snapshot of the system’s dynamical state. The output together with the parameters and boundary conditions (no-flux) defines a complete current dynamical state of the spiral wave dynamics. We then used the diffusion model outputs as initial states for the biophysical model defined in eqs. (1-2) and initiated 5, 000 simulations with these diffusion-generated initial conditions with identical model parameters as during training data generation and measured the time until each simulation self-terminated over the ensemble of simulations, see section III F.

Task 4: Generation of Scroll Waves in Heart-shaped Geometries

We trained a diffusion model to generate scroll waves in bi-ventricular-shaped geometries (Task 4), similarly as described in section II B 3 and as shown in Fig. 4. Both the shape and the wave pattern were generated by the diffusion model simultaneously. This means that the diffusion model outputs an arbitrary bi-ventricular geometry as well as a corresponding anisotropic scroll wave pattern, the anisotropy reflecting the underlying fiber architecture. The generation was unconditional as described in the previous section II B 3. The simulated training data, see section II A, consists of pointclouds of ($\sim 32, 000$) vertices $p(\vec{x}_i)$ located within bi-ventricular heart shapes and scalars representing the excitatory variable u_i per vertex with index i , see Fig. 5. We downsampled the data to 16, 000 points and used Point-Voxel Diffusion [28] trained on 5, 000 training samples obtained from the simulations. We trained the model to output 16, 384 points (with a latent dimension of 512).

Task 5: Generation of Spiral Wave Dynamics and Integration of their Spatio-Temporal Evolution

We trained a diffusion model to calculate an immediate future time step of a given spatio-temporal excitation wave pattern (Task 5):

$$(u, r)(\vec{x}, t) \rightarrow (\tilde{u}, \tilde{r})(\vec{x}, t + \tau) \quad (10)$$

where (u, r) are the dynamic variables from eqs. (1-2) and τ is an infinitesimal temporal increment or the integration time step. In other words, we trained a diffusion

model to be able to evolve cardiac excitation wave dynamics. More precisely, we trained the model to predict the next 5 time steps from the previous 5 time steps of the dynamics, resulting in a temporal integration scheme that updates a brief spatio-temporal pattern instead of a static spatial pattern. We found this approach to be more stable than auto-regressively integrating the dynamics, e.g. updating the dynamics one time step at a time and predicting the next time step from the previous 5 time steps. With this spatio-temporal integration eq.(10) corresponds to:

$$(u, r)(\vec{x}, t_{-4}, \dots, t_0) \rightarrow (\tilde{u}, \tilde{r})(\vec{x}, t_1, \dots, t_5) \quad (11)$$

where t_{-4}, \dots, t_0 are the 4 previous and the current time steps and t_1, \dots, t_5 are the next 5 future time steps, see Fig. 6A). We trained and evaluated the model with 15,000 and 5,000 samples, respectively, showing two-dimensional spiral wave dynamics with the simple and complex parameter sets from section II B 2, see Fig. 6B,C).

Task 6: Parameter-specific Generation of Spiral Waves

We trained a diffusion model to generate parameter-specific spiral wave dynamics (Task 6), as shown in Fig. 8:

$$(\xi(x, y), k, \epsilon_0) \rightarrow (\tilde{u}, \tilde{r})(x, y, t_1, t_4, t_7, t_{10}, t_{13}) \quad (12)$$

where k and ϵ_0 are parameters of the biophysical model in eqs.(1-2) and (\tilde{u}, \tilde{r}) is a short sequence of 5 predictions of the dynamical state of the spiral wave patterns at future times $t_1, t_4, t_7, t_{10}, t_{13}$ given in simulation time steps, see detailed explanation below. The diffusion model generates spiral wave patterns from the initial noise $\xi(x, y)$ and we refer to this generation process as 'conditioned by the parameters k and ϵ_0 '. The model generates a sequence of 5 subsequent spiral wave patterns for validation purposes, see section III G.

We generated a training dataset in which we varied the parameters k and ϵ_0 systematically and initiated spiral wave dynamics with these parameters for 20 different parameter pairs (k, ϵ_0) , see Fig. 8A,B). We ran 200 simulations over the 20 parameter pairs on the grid $k = [7, 7.5, 8, 8.5, 9]$ and $\epsilon_0 = [0.0001, 0.001, 0.003, 0.015]$ with 10 simulations per parameter combination, and selected data from 15 of the 20 parameter sets to train the model and the remaining 5 for testing, as shown in Fig. 8A,B). We then conditioned the diffusion model by concatenating the parameters to the initial noisy distribution $\xi(x, y)$, adding two channels to the input of the underlying U-Net ($2 \times 128 \times 128$ pixels). Aside from the parameter conditioning, the generation was unconditioned allowing the diffusion model to dream up any spiral wave pattern, as described in section II B 3.

To test the specificity of the parameter-specific generations, we set up the training and prediction process as follows: for each simulation, we extracted 150 frames

and grouped every 15 frames into one training sample $\{(u, r)_1, \dots, (u, r)_{15}\}$. Of these 15 frames, we used only 5 frames per training sample, subsampling the data in time by a factor of 3: $\{(u, r)_1, (u, r)_4, (u, r)_7, (u, r)_{10}, (u, r)_{13}\}$. Using this data as the target during training, the diffusion model was trained to predict a short spatio-temporal sequence of spiral wave dynamics consisting of 5 frames with an offset of 3 frames, see eq.(12). We then evaluated whether the diffusion model can generate different parameter-specific dynamics by loading the first predicted dynamical state $(\tilde{u}, \tilde{r})_1$ created with a specific parameter pair (k^*, ϵ_0^*) and evolving it using the biophysical model (integrating the PDEs) for 15 simulation time steps using either the same parameter pair (k^*, ϵ_0^*) or a different one (k, ϵ_0) . We repeated this process with all 20 parameter pair combinations and compared the 5-th diffusion-generated frame $(\tilde{u}, \tilde{r})_{13}(x, y)$ to the output of the simulation at time step 13 by calculating the error (RMSE) between the two frames, see Fig. 8D).

C. Training Details

The networks were trained using the Adam [43] optimizer with a learning rate of 10^{-4} for the bulk prediction tasks and 10^{-3} all other tasks. We used a batch size of 8 for the bulk prediction tasks and a batch size of 32 for all the other tasks. All neural network models were implemented in PyTorch [38]. Training and reconstructions were performed on a NVIDIA RTX A5000 graphics processing unit (GPU).

Model	Trainable Parameters	Training Time
Task 1	965,266,792	9 days
Task 2	62,640,193	1.5 days
Task 3	113,673,219	1.5 days
Task 4	31,092,676	1 day
Task 5	62,644,805	1.5 days
Task 6	250,430,474	4 days
Classification	11,689,512	5 min

TABLE II. Different model sizes (trainable parameters) and training times used in this study. Training was performed on a single NVIDIA RTX A5000 GPU.

D. Evaluation

We evaluated the diffusion models accuracies using the root mean squared error (RMSE), the mean absolute error (MAE), or the multi-resolution perceptual error (MR) [41] depending on the model and task. We computed the errors per frame, averaging over all frames of a separate evaluation dataset that was not part of the training dataset. While RMSE and MAE correspond to a measure of the average difference per pixel, the perceptual error is a measure for the similarity of two patterns as it

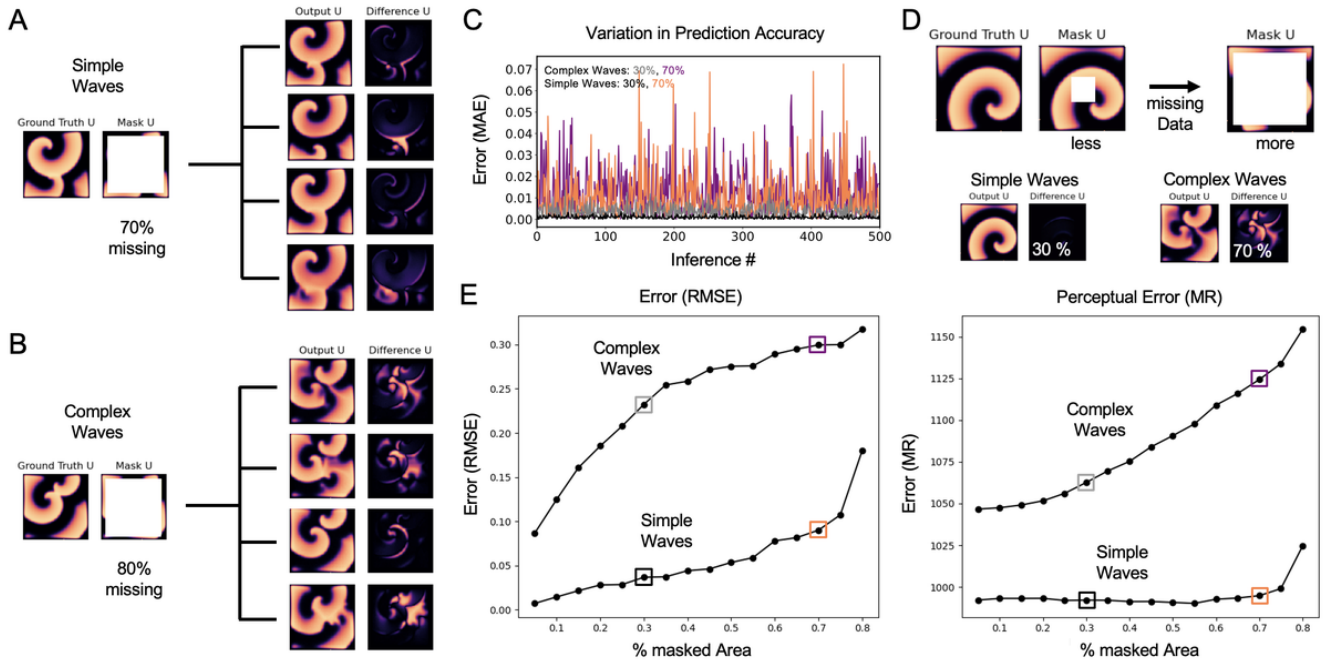


FIG. 4. Hallucination of diffusion model during inpainting of electrical spiral wave dynamics. **A** The diffusion model predicts missing data inside a square region (white) at the center of the medium. With most of the data missing (70%), the diffusion model dreams up wave patterns which look convincingly like spiral wave patterns but deviate substantially from the ground-truth: 4 repetitive predictions for the same interpolation task. **B** The effect becomes more severe with more complex waves and fewer data (80% missing), see also panel D and Supplementary Video 2. **C** The model generates significantly different output when the same prediction task is performed repeatedly (500 times, black: simple waves with 30%, gray: simple waves with 30%, orange: complex waves with 70%, pink: complex waves with 70% missing data, respectively). **D** Combinations of less vs. more missing data (30% vs. 70%) and simple and complex waves. **E** Average prediction error (RMSE vs. perceptual MR) with increasing percentage of missing data. Hallucination is minimal with simpler wave patterns and 10-30% missing data and increases steeply with complex wave patterns. The perceptual error indicates a higher agreement between inpainted and ground-truth patterns which is not reflected by RMSE, see also Fig. 3.

calculates the difference on the embedding in the network [41], see also Fig. 4 and section III B.

III. RESULTS

A. Reconstruction of Three-Dimensional Scroll Wave Dynamics from Surface Observations

Measuring electrophysiological wave phenomena beneath the heart surface is a challenge in cardiovascular research and diagnostics. Catheter electrodes or optical mapping provide only data from the surface of the heart and intramural measurements from within the heart muscle using, for instance, plunge needle electrodes provide only sparse information. To address this challenge, various numerical methods were introduced which aim at reconstructing transmural wave patterns from observations of the dynamics on the tissue’s surface [29, 30, 44, 45]. The numerical reconstructions are particularly relevant in the context of tachyarrhythmias, such as ventricular or atrial fibrillation, as they may provide a better understanding of the underlying three-dimensional spatio-

temporal organization of the electrical waves within the heart muscle. Recently, Lebert et al. [29] and Stenger et al. [30] demonstrated that convolutional encoding-decoding neural networks (different U-Net-types) can be used to reconstruct three-dimensional scroll wave dynamics inside a thick bulk-shaped excitable medium from two-dimensional observations of the dynamics on the top and/or bottom surfaces (representing the epi- and endocardium). At the same time, Stenger et al. demonstrated this briefly also with a diffusion model [30]. However, several aspects of the deep learning-based reconstructions remain underexplored, in particular with the diffusion-based approach. The deep learning-based reconstructions assume scroll waves inside the tissue as the neural networks are trained with thousands of corresponding pairs of three- and two-dimensional data of scroll waves and observations thereof. Therefore, the training data implicitly restricts the approach to a particular distribution of data and its characteristics (specific electrophysiological model that produces waves with a particular shape, isotropic vs. anisotropic wave patterns, wavelength relative to medium thickness), and the approach is task-specific (single- vs. dual-surface observations).

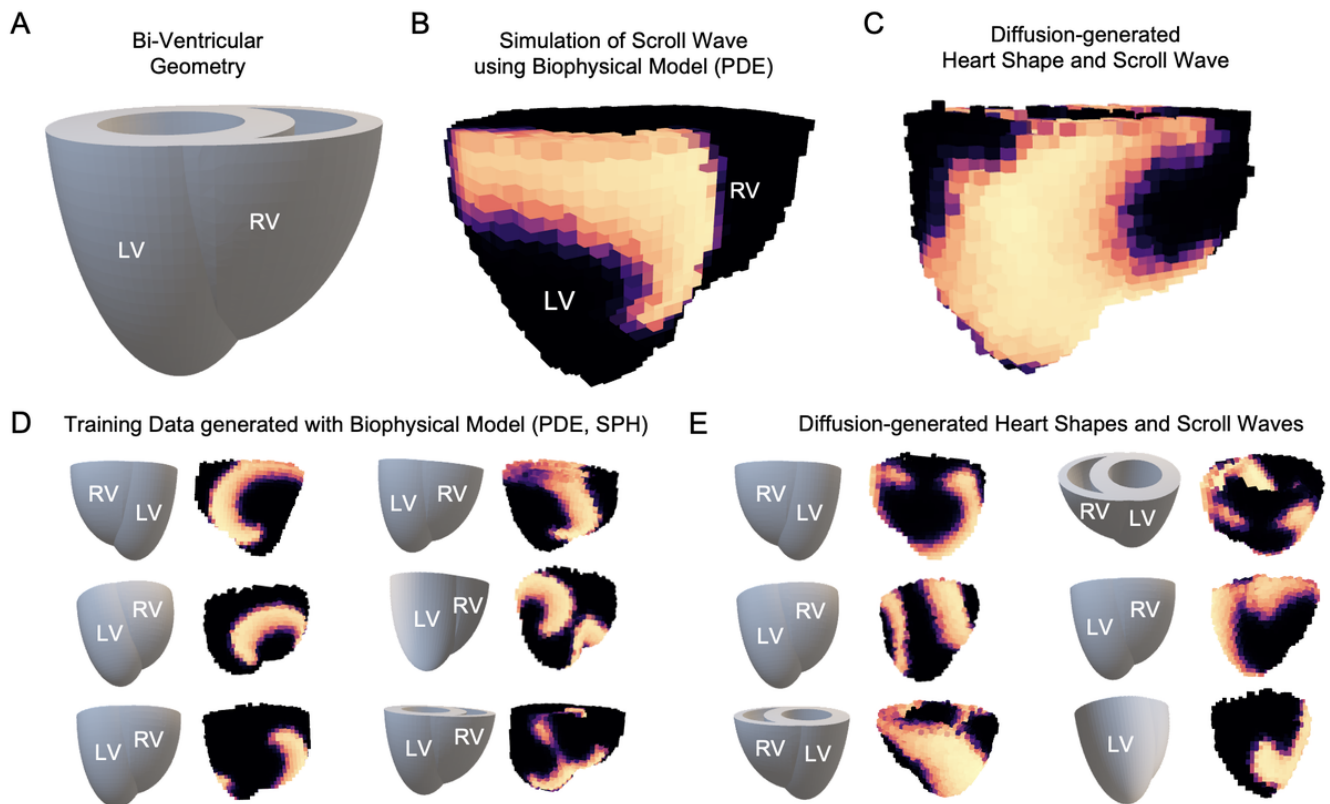


FIG. 5. Diffusion-based modeling of reentrant electrical waves in heart-shaped bi-ventricular geometries. **A** Bi-ventricular template geometry, which was deformed to create 1,000 unique geometries for the training data generation, as described in [29]. **B** Example of three-dimensional electrical scroll wave in bi-ventricular heart model simulated using a biophysical model (Aliev-Panfilov), see eqs.(1)-(2), integrated using SPH-method [32, 33], see section II A. The data was voxelized and volume-rendered. **C** Diffusion-generated electrical scroll wave in bi-ventricular heart shape with muscle fiber anisotropy. Both the geometry and the wave pattern were generated simultaneously. **D** The training data consists of 5,000 training samples showing scroll wave patterns. Each simulation consists of 32,000 particles, the data was subsampled to 16,000 particles for training. **E** Further examples of diffusion-generated electrical scroll waves in bi-ventricular heart shapes. The diffusion model generates a bi-ventricular shape (each shape different but only template geometry shown) as well as a full state with both dynamic variables $(u, r)(\vec{x})$. The scroll wave patterns are anisotropic following the underlying ventricular muscle fiber organization.

Here, we compared a diffusion model to a U-Net model for predicting three-dimensional scroll waves inside an anisotropic bulk-shaped excitable medium, see Figs. 2-3. Both models predict a three-dimensional scroll wave pattern from a short sequence ($N = 5$) of two-dimensional observations on either only the top (single-surface mode) or ii) both the top and bottom surface layers (dual-surface mode) of the bulk, as in [29], see also Fig. 3. The bulk is completely opaque and thick enough to sustain three-dimensional scroll wave dynamics ($128 \times 128 \times 40$ voxels, 1-2 wavelengths), see Fig. 2. Fig. 2A) shows the generative denoising process of the diffusion model. Interestingly, the rough shape of the scroll wave pattern is already captured early in the denoising process, while later stages enhance finer structures. We found that both diffusion and U-Net produce sufficiently accurate reconstructions, the diffusion model slightly outperforming U-Net, see Fig. 3. In [30] it was found that diffusion performs substantially better than U-Net with long

observations of the surface (32 snapshots). Here, we used fewer observations (only 5 snapshots) which likely causes this discrepancy. Another methodological difference to [30] is that our diffusion model predicts the bulk at once and not layer by layer. Fig. 2B) shows a comparison of the ground-truth scroll wave pattern with predictions obtained with i) diffusion, ii) U-Net, and iii) diffusion refining the U-Net output, see section II B 1 for details. While U-Net reconstructions become fuzzier with increasing depth, diffusion maintains the shape and smoothness or overall look of the scroll waves throughout the bulk. This is also reflected by the perceptual error, see also section III B. Unlike in [30], our model produces scroll wave patterns without residual noise. However, even though the visual impression suggests otherwise, we find on average no dramatic improvement of the reconstruction accuracy (RMSE) with diffusion over U-Net, see Fig. 3. Upon closer inspection, one notices that diffusion produces minor mismatches at deeper layers (white

boxes in Fig. 2B), suggesting that its output looks better but is not necessarily more accurate than with U-Net, see also section III B. We tested whether guiding the diffusion model with the output from the U-Net model could mitigate these issues. However, refining the U-Net output with diffusion increases the reconstruction accuracy only marginally, see Fig. 3.

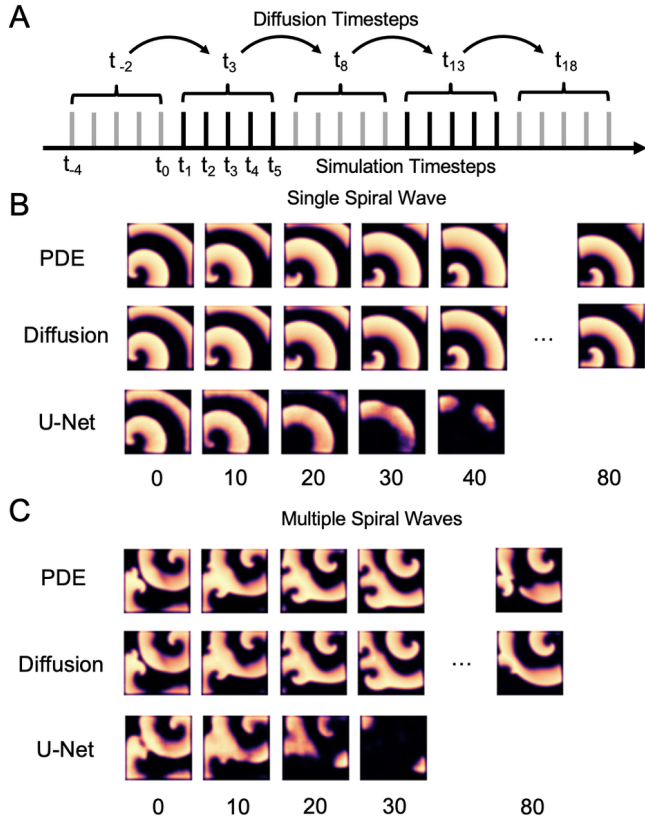


FIG. 6. Data-driven modelling of spiral wave dynamics using diffusion models. **A** Spatio-temporal prediction (Task 5) of 5 frames from previous 5 frames, see section II B 5. **B,C** Comparison of ground-truth data (GT) simulated with biophysical model (finite differences) and data-driven methods (Diffusion vs. U-Net) to evolve the wave pattern. With a single spiral wave, the output of the diffusion model is visually indistinguishable from the ground-truth for many rotations, while U-Net quickly fails to sustain the wave pattern. With more complicated wave patterns, the diffusion models begins to deviate from the biophysical model after 2-3 spiral rotations (80 time steps).

B. Hallucination during Inpainting of 2D Spiral Wave Dynamics

Generative models are known to hallucinate, which means that they may generate output that looks, sounds or reads convincing but is inaccurate. For example, recent large language models (LLMs) are known to confidently present made-up knowledge as if it was factual.

In computer vision, diffusion models may generate unexpected scenes which are abstract and not part of human day-to-day experience. While it is easy to identify hallucination in diffusion-generated visual scenes, it is not necessarily obvious with spiral or scroll wave patterns when they include hallucinations, see also section III D. In Fig. 2, the diffusion-generated reconstructed scroll wave patterns at midwall look convincing and can be misinterpreted as accurate solutions, but they are just as inaccurate as the output from the U-Net model.

We explored this hallucinating behavior further in a two-dimensional inpainting task of spiral wave dynamics, see Fig. 4, and can confirm that hallucination occurs, particularly when the task is insufficiently constrained, see also Supplementary Video 2. We varied the size of a square region at the center of the medium, within which the diffusion model was tasked to interpolate the missing spiral wave pattern from the surrounding data, see section II B 2 for details. Hallucination is minimal with a small square, which is reflected by the error (RMSE) on the left sides of the graphs in Fig. 4E). However, we observed that the diffusion model comes up with many different spiral wave patterns for the same task when the square region is large, see Fig. 4A,B) and Supplementary Video 2. The graph in Fig. 4C) shows the variation of the diffusion model output when the same task is repeated over and over (500 times with simple vs. complex waves and 30% vs. 70% missing data respectively). The variation in the output as quantified by the error (MAE) between the ground-truth and the individual predicted spiral wave pattern is particularly large with 70% missing data. Hallucination becomes also stronger when the wave dynamics are more complicated (we tested two parameter sets, see Table I), compare panels A,B) and the upper and lower curves in E) (average error calculated over 500 unique samples per data point). In Fig. 4E) we compared the root mean squared error (RMSE), which reflects the pixel-wise congruency of the ground-truth and the predicted pattern, with a perceptual error (MR), which reflects similarities or differences in the patterns independently from spatial mismatches (as it is calculated on the embedding of the pattern). The perceptual error indicates that with simple waves the variations in the output of the diffusion model are small regardless of the size of the masked area. In other words, differences in the waves only correspond to slight spatial mismatches (which cause high RMSE), while the wave shapes are very similar qualitatively. The spikes in C) (with 70%), on the other hand, correspond to large qualitative changes of the wave pattern which occur occasionally with both complex and simple waves. Our data suggests that the diffusion model hallucinates if it has the freedom to generate many possible fitting solutions to a problem, that hallucination can be associated with qualitative changes in the topology of the wave pattern, and that hallucination can be mitigated by sufficiently constraining the task that the diffusion model is supposed to perform.

C. Generation of Reentrant Scroll Waves in Heart-shaped Geometries

Fig. 5A-D) shows three-dimensional scroll waves in bi-ventricular heart shapes that were generated using the diffusion model detailed in section II B 4. The generative process was completely unconstrained and the model generates any scroll wave pattern it can come up with. Exemplary solutions of the biophysical model and the diffusion model, which are shown in panels C,D) respectively, are visually indistinguishable from each other, see also Fig. 7 and section III D. The diffusion model generates randomly-shaped bi-ventricular heart geometries and corresponding electrical scroll wave patterns simultaneously. The scroll wave patterns are anisotropic because the training data was generated in an anisotropic bi-ventricular fiber architecture which implicitly defines anisotropy during the generations. The data was generated in a pointcloud-based fashion, see section II B 4, and was voxelized for visualization purposes. The bi-ventricular template geometry in panel B) was deformed randomly during the training process generating a variety of shapes and the diffusion model comes up with similar shapes during the generative process, see also [31]. Even though the diffusion model generates only a single scroll wave pattern $u(\vec{x}, t)$, it is easy to imagine how this pattern could also be evolved over time $u(\vec{x}, t_1, t_2, \dots)$ as described in section III E and shown in Fig. 6.

D. Visual Similarity of Diffusion- vs. PDE-generated Spiral Waves

Diffusion-generated 'fake' spiral waves are visually indistinguishable from real spiral wave patterns simulated with the biophysical model and partial differential equations (PDEs), see Fig. 7A,B). Each panel shows 4×4 randomly chosen, representative examples of spiral wave patterns simulated with PDEs or diffusion, respectively. The diffusion-generated spiral wave patterns in B) were generated using the diffusion model described in section II B, which was trained on spiral wave patterns obtained with a fixed parameter set, shown in A). We found it impossible to distinguish the two patterns visually (we tested this systematically with different lab members). Despite the visual similarity, a ResNet18 [46] classifier fine-tuned on the two classes of images in panels A,B) is able to distinguish the two groups of spiral wave patterns with an accuracy of 99.7% (separate training and validation/test datasets). This may be due to invisible artifacts from the denoising process or the capability of CNNs to learn minute differences between classes. This is well explored, and was in part the motivation behind the joint generator-discriminator training process of GANs. Each specific diffusion-generated spiral wave image was generated from a random distribution of noise $\xi(x, y)$, which was the only information that guided the generation process, see also Supplementary Video 3.

E. Generative Diffusion-based Simulation of Electrical Wave Dynamics

Electrical impulse propagation in the heart is usually simulated by integrating or evolving a biophysical model consisting of partial differential equations in space and over time, e.g. by using the finite difference or finite element methods to solve a set of partial differential equations. Here, we show that, alternatively, diffusion-based data-driven modeling can be employed to simulate excitation waves in cardiac tissue. We used the simulated spiral wave data (from Task 2 and Fig. 4) to train a diffusion model in such a way that it can calculate the next dynamical state given a current state of wave dynamics $\chi_t : (u, r)(x, y, t)$ enabling it to evolve the dynamics $\chi_t \rightarrow \chi_{t+1}$, see section II B (Task 5). Fig. 6B,C) shows the ground-truth (GT) spiral wave patterns for up to 80 simulation time steps and the corresponding evolved spiral wave patterns predicted either with our diffusion model or a correspondingly trained U-Net model. While the dynamics quickly degenerate with U-Net, the diffusion model successfully sustains and evolves the dynamics over a very long time. The ability to sustain the wave pattern is likely related to diffusion models being able to learn and mimic shapes. The diffusion model produces spiral waves with either stable or meandering cores which exhibit breakup and (self-) interactions. With the single spiral wave in Fig. 6B) the diffusion model's output matches the biophysical model's output for many rotations, see Supplementary Video 4. Eventually, the original (ground-truth) dynamics diverge from the diffusion-generated dynamics. However, this divergence is to some extent to be expected as the dynamics would also diverge with, for instance, two different integration methods (forward Euler vs. third-order methods) or integration time steps even with the same biophysical model. With the more complex spiral wave dynamics in Fig. 6C) the diffusion output diverges rapidly within less than 2 rotations of the spiral wave pattern, see Supplementary Video 5. Interestingly, the diffusion model appears to produce more stable wave dynamics (less wavebreak), which could be associated with a bias in the training data towards stable waves. We found that the diffusion-based integration works best when updating multiple time steps at a time (e.g. $t_{-4, \dots, 0} \rightarrow t_{1, \dots, 5}$), see also Fig. 6A), instead of updating the dynamics one time step at a time $t_1 \rightarrow t_2$ as, for instance, with the forward Euler integration method. The multi time step integration works also better than auto-regressively predicting the next frame while including previous predictions. Updating the dynamics in a 128×128 pixel simulation domain takes 1.1 ms on a NVIDIA A5000 GPU. Together with our findings in III C, the data suggests that the generative diffusion-based integration of spatio-temporal dynamics could also be used to evolve scroll wave dynamics in three-dimensional heart-shaped geometries.

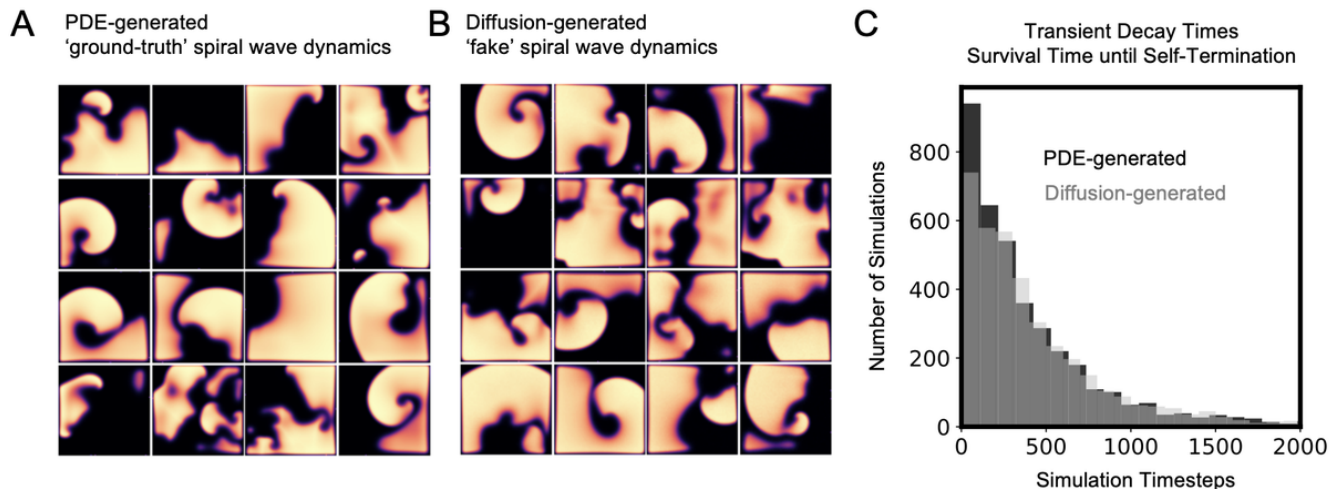


FIG. 7. Comparison of spiral wave dynamics generated in computer simulations using a biophysical model (ground-truth) and 'fake' diffusion-generated spiral wave dynamics. **A,B** The two datasets are visually indistinguishable from each other. **C** Distribution of self-termination times measured for an ensemble of 5,000 randomly initiated spiral wave dynamics and 5,000 diffusion-generated spiral wave dynamics. Most spiral wave dynamics self-terminated after 1,000 simulation time steps, regardless of whether they were simulated in a conventional fashion using partial differential equations or initiated by diffusion.

F. Transient Behavior of Diffusion-generated Spiral Waves

Spiral wave dynamics are known to eventually self-terminate over time with an exponential decay rate [42]. Fig. 7C) shows that diffusion-generated spiral wave patterns also self-terminate following the same law with approximately the same decay rate. The decay rates of the original simulated spiral wave dynamics (black) and the diffusion-generated spiral wave dynamics (gray), which were initiated using the $(u, r)(x, y)$ outputs from the diffusion model and evolved with the biophysical model, are close to identical, see section II B (Task 3) for details. The two distributions of survival times calculated from the two ensembles of dynamics indicate that most spiral wave dynamics self-terminate before 500 simulation time steps and that only few survive longer than 1,500 simulation time steps. The slight discrepancy between the two distributions towards short survival times may result from the way the measurement was performed: the diffusion model was trained with data sampled from a particular sampling time step including the previous 300 time steps, while the PDE-generated distribution was calculated from an ensemble of simulations measured only at exactly that particular sampling time step. The data suggests that the diffusion-generated spiral wave patterns stem from the same part of the chaotic attractor of the dynamics. We created training samples from that part of the attractor, trained the diffusion model with this particular distribution of samples and the diffusion model generates new spiral wave patterns and reproduces the same distribution of spiral wave patterns, which then, when used as initial conditions and evolved further using the biophysical model, collectively exhibit the same

self-termination rates. The diffusion model appears to capture the underlying parameter-specific characteristics of the dynamics.

G. Parameter-specific Generation of Spiral Wave Dynamics

The diffusion model described in section II B 6 can generate parameter-specific spiral wave dynamics when given a set of parameters as input, see Fig. 8. This means that the generative process can be guided by parameters to produce spiral wave dynamics with specific properties which would similarly arise with a biophysical model with the same parameters. Spiral wave dynamics can be very different depending on the chosen model parameters. For instance, spiral wave cores can drift or be stationary depending on the parameters, see for example Fig. 9 in [47]. Here, the Aliev-Panfilov model produces regimes with fewer or more spiral waves when varying the parameters k and ϵ_0 in eqs. (1)-(2), see Fig. 8A,B). Our diffusion model reproduces these different parameter-specific regimes when conditioned with the respective parameters during the generation process, see Fig. 8C,E). Importantly, the diffusion model can generate parameter-specific spiral wave dynamics even if it was not trained with the specific parameter combination. We split the simulation data in parameter space into training and test data, as shown in Fig. 8 A,B), and some of the generations in C) were obtained with parameter combinations not included during the training process. We verified that these diffusion-based generations correspond to parameter-specific dynamics as follows: 1) We let the diffusion model generate a short sequence

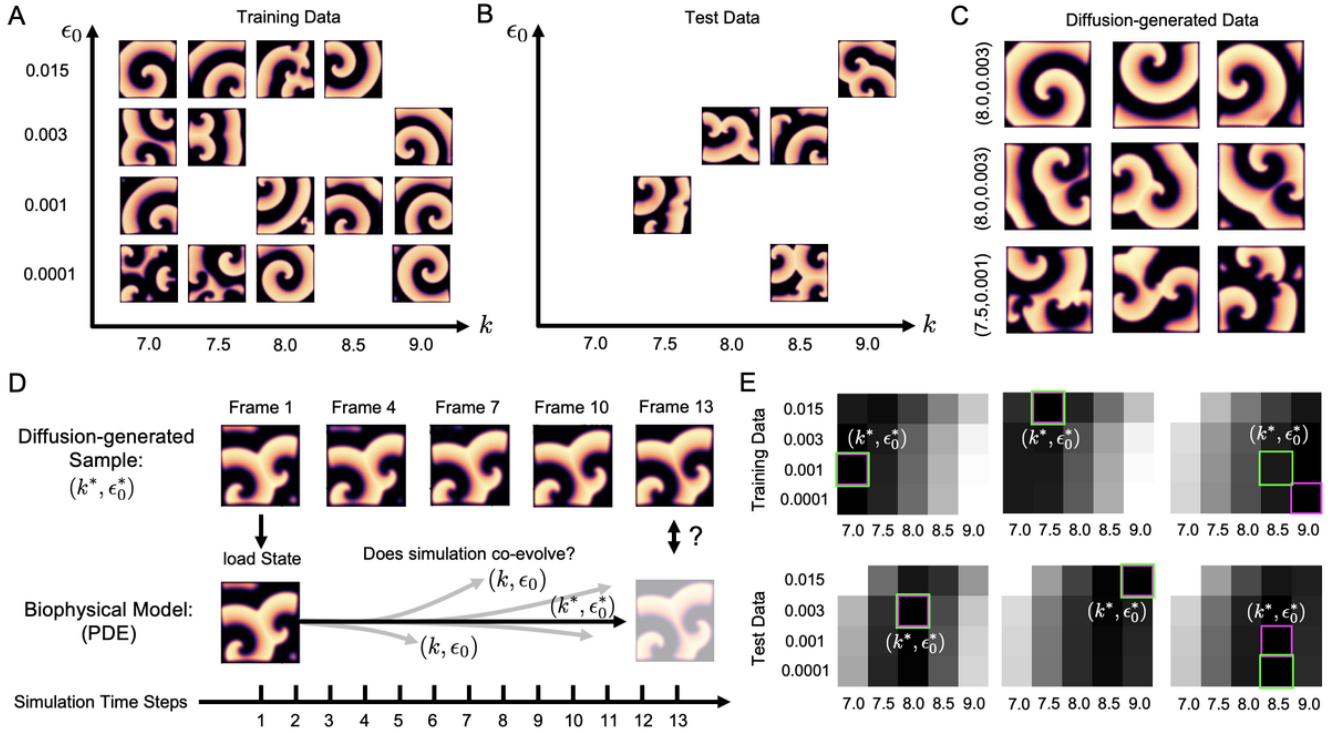


FIG. 8. Parameter-specific generation of spiral wave dynamics using diffusion generative modeling. **A** The diffusion model was trained on spiral wave data simulated with different parameters, varying the parameters k and ϵ_0 in eqs. (1)-(2). Some parameter combinations produce more and some less spiral waves. **B** Test data which was left out of the training data. **C** Examples of diffusion-generated spiral wave dynamics with parameter combinations $(k, \epsilon_0) = \{(7, 5.0.001), (8, 0.003)\}$. With the same parameter combination, the waves can look very different. Vice versa, with different parameter combinations, the waves can look very similar. **D** Scheme to test whether diffusion-based generations are parameter-specific. Top: Sequence of 5 diffusion-generated frames. Overloading of first frame into biophysical model as initial state for testing whether state co-evolves, see section III G for details. The biophysical model co-evolves the closest (black arrow) when parameters of the simulation match the parameters (k^*, ϵ_0^*) with which the diffusion generation was conditioned. **E** Confirmation that generations are parameter-specific: the error (RMSE) between simulated and diffusion-generated output (frame 13 / 5) is the lowest for matching or close parameter combinations $(k, \epsilon_0) \approx (k^*, \epsilon_0^*)$. Green box: parameter combination (k^*, ϵ_0^*) of diffusion-generated data, see top in panel D. Pink box: combination producing minimum mismatch (RSME, black: low, white: high) between simulation and diffusion-generated sequence (k and ϵ_0 combinations used for simulation).

of 5 frames $\{(\tilde{u}, \tilde{r})_1, (\tilde{u}, \tilde{r})_4, (\tilde{u}, \tilde{r})_7, (\tilde{u}, \tilde{r})_{10}, (\tilde{u}, \tilde{r})_{13}\}(x, y)$ with a parameter combination (k^*, ϵ_0^*) as conditioning, see Fig. 8D). The frames correspond to every third frame in a sequence of 15 frames, as described in section II B 6. 2) Then we used the first predicted frame $(\tilde{u}, \tilde{r})_1(x, y)$ to initialize the biophysical model together with either i) the same parameter combination (k^*, ϵ_0^*) or ii) a mismatching parameter combination (k, ϵ_0) from $k \in [7.5, \dots, 9.5]$ and $\epsilon_0 \in [0.0001, \dots, 0.015]$. 3) Then we evolved this state by integrating the PDEs of the biophysical model in space and over the next 15 time steps. Lastly, we compared the 5-th frame generated with the diffusion model to the 13-th time steps simulated with the biophysical model and calculated the error (RMSE) between them. This way we could check whether the diffusion model and the biophysical model co-evolve, and whether the diffusion model generates a dynamical state that, when evolved over time using the biophysical model, evolves as expected with that parameter combination and matches

the diffusion model's output at a later time. We chose a short simulation interval of 15 time steps to minimize the influence of the model's intrinsic dynamics. We repeated this procedure for all 20 combinations of (k, ϵ_0) to check whether the biophysical model co-evolves best with the right parameter combination (k^*, ϵ_0^*) and found that the error is minimal when the parameters are close or match $(k, \epsilon_0) = (k^*, \epsilon_0^*)$, see Fig. 8E). We see this as an indication that the parameter-specific output of the diffusion model is representative of the simulation data at that parameter combination. In other words, this means that the diffusion model generates spiral wave patterns that the biophysical model also produces with these parameters. We would expect the minimum to vary and not be located at $(k, \epsilon_0) = (k^*, \epsilon_0^*)$ if the output of the diffusion model was more arbitrary and unspecific. The fact that the minimum does not always strictly occur at $(k, \epsilon_0) = (k^*, \epsilon_0^*)$ is likely related to very similar dynamics for close parameter combinations, see also Fig. 8C).

Overall, the diffusion model appears to be able to interpolate in parameter space and generate valid parameter-specific dynamics in between parameter combinations it was trained on. This suggests that diffusion models do not need to be trained meticulously on all possible parameter combinations and can yet generate wave dynamics for many more parameter combinations than just the ones they were trained on. Note that all tested parameter combinations except ($k = 9.0, \epsilon_0 = 0.015$) lie in between the training parameter combinations.

IV. DISCUSSION

Generative modeling provides many promising applications in the biological and biomedical sciences. Here, we demonstrated that denoising diffusion probabilistic models can be used to model waves of electrical excitation in cardiac tissue. Diffusion models can be used to reconstruct or create parameter-specific wave patterns, and, most importantly, simulate electrical wave propagation in a data-driven manner. In other words, diffusion models can learn to evolve cardiac wave dynamics from previously seen data without knowledge about the underlying physics. Therefore, they could potentially be used to create a data-driven model of the heart's electrophysiological system from measurement data. We found that diffusion models not only generate electrical wave dynamics that look like and are visually indistinguishable from simulated wave dynamics, but the diffusion-generated dynamics also preserve some of the inherent characteristics of the original dynamics. For instance, we found that diffusion-generated spiral wave dynamics exhibit the same self-termination statistics as their counterparts in excitable media, see section III F.

While we have some confidence that the diffusion-generated waves are indeed legitimate solutions, we also remain cautious and further research is needed to confirm whether diffusion models provide a valid and robust alternative modeling approach to conventional biophysical modeling. At this point, we cannot rule out that diffusion models merely emulate rather than simulate spiral wave dynamics. This concern is particularly critical when the dynamics are chaotic and sensitive to slight physical perturbations or differences in the numerical integration. We evolved both simpler and more complicated spiral wave dynamics, and while the diffusion model generated plausible looking simpler spiral wave dynamics for very long times (in contrast to U-Net) which co-evolved over a reasonable period of time with the ground-truth dynamics (keep in mind that even different solvers would lead to diverging results), the more complicated spiral wave dynamics diverged very quickly from and exhibited less wavebreak than their ground-truth counterpart. The latter observation could be an indication that bias in the training data influences the behavior of the dynamics in a non-deterministic way.

A major concern with diffusion models is their ability

to hallucinate. Hallucination is an inherent property of generative modeling and a feature and bug at the same time. Diffusion models can generate a continuum of outputs of which some are made up and false. The main issue is that the false output is hard to identify as diffusion models excel at learning the data distribution and generating realistically looking data points from this distribution. This raises concerns over the applicability of diffusion models in healthcare, where they could produce misleading output which could lead to an incorrect diagnosis or treatment. Here, we found that the extent to which diffusion models hallucinate is related to how much the task that the network is supposed to perform is constrained. If the problem is more constrained, then the space of possible solutions becomes smaller and there is less potential for hallucination (e.g. when evolving dynamics). Therefore, sufficiently constraining diffusion models as well as developing methods to quantify and mitigate hallucination is essential. Nevertheless, the perceived weaknesses with regard to hallucination can also be a major advantage in other situations: diffusion models excel when tasked to generate a starting point in underconstrained tasks, and therefore they could serve as a powerful prior for difficult cardiac modeling or reconstruction tasks.

Overall, despite the potential drawbacks, diffusion models are a promising tool with many potential applications in cardiac research and diagnostics. Diffusion models can in principle generate parameter- or even model-specific (scroll) wave dynamics in three-dimensional heart-shaped geometries, suggesting that they could be used to simulate atrial or ventricular fibrillation in an individualized segmentation of a patient's heart while also integrating measurement data (e.g. catheter mapping data) and generating patient- or disease-specific wave dynamics. In particular, diffusion models offer the possibility to learn different integration time scales, perform simulations at arbitrary resolutions, and skip the tedious part of finding the right initial conditions for simulating such dynamics as they can readily generate spiral and scroll wave patterns instantaneously.

V. CONCLUSIONS

We demonstrated that denoising diffusion probabilistic models (DDPMs) can be used for generating electrophysiological wave patterns in cardiac tissue. More specifically, they can be used for recovering missing data, evolving spatio-temporal dynamics, or generating specific parameter-dependent dynamics, among other tasks. The diffusion-generated waves are visually indistinguishable from and behave as waves simulated with biophysical models. However, diffusion models tend to hallucinate with insufficient constraining and require significant computational resources during training. In the future, diffusion models could be used for data-driven modeling of various physiological phenomena in the heart.

-
- [1] V. I. Krinsky and H. L. Swinney, *Waves and Patterns in Chemical and Biological Media* (The MIT Press, 1991).
- [2] A. Winfree, Electrical turbulence in three-dimensional heart muscle, *Science* **266**, 1003 (1994).
- [3] S. Alonso, M. Bär, and B. Echebarria, Nonlinear physics of electrical wave propagation in the heart: a review, *Reports on Progress in Physics* **79**, 096601 (2016).
- [4] W.-J. Rappel, The physics of heart rhythm disorders, *Physics Reports* **978**, 1 (2022), the physics of heart rhythm disorders.
- [5] A. M. Pertsov, R. Davidenko, J. M. Salomonsz, W. T. Baxter, and J. Jalife, Spiral waves of excitation underlie reentrant activity in isolated cardiac muscle, *Circulation Research* **72**, 631 (1993).
- [6] R. A. Gray, J. Jalife, A. Panfilov, W. T. Baxter, C. Cabo, J. M. Davidenko, and A. M. Pertsov, Nonstationary vortexlike reentrant activity as a mechanism of polymorphic ventricular tachycardia in the isolated rabbit heart, *Circulation* **91**, 2454 (1995).
- [7] P. Pathmanathan and R. A. Gray, Filament dynamics during simulated ventricular fibrillation in a high-resolution rabbit heart, *BioMed Research International* **2015**, 10.1155/2015/720575 (2015).
- [8] J. Christoph, M. Chebbok, C. Richter, J. Schröder-Schetelig, P. Bittihn, S. Stein, I. Uzelac, F. H. Fenton, G. Hasenfuss, R. J. Gilmour, and S. Luther, Electromechanical vortex filaments during cardiac fibrillation, *Nature* **555**, 667 (2018).
- [9] I. Uzelac, S. Irvanian, N. K. Bhatia, and F. H. Fenton, Spiral wave breakup: Optical mapping in an explanted human heart shows the transition from ventricular tachycardia to ventricular fibrillation and self-termination, *Heart Rhythm* (2022).
- [10] F. Fenton and A. Karma, Vortex dynamics in three-dimensional continuous myocardium with fiber rotation: Filament instability and fibrillation, *Chaos: An Interdisciplinary Journal of Nonlinear Science* **8**, 20 (1998).
- [11] O. Berenfeld and A. M. Pertsov, Dynamics of intramural scroll waves in three-dimensional continuous myocardium with rotational anisotropy, *Journal of Theoretical Biology* **199**, 383 (1999).
- [12] Z. Qu, J. Kil, F. Xie, A. Garfinkel, and J. N. Weiss, Scroll wave dynamics in a three-dimensional cardiac tissue model: Roles of restitution, thickness, and fiber rotation, *Biophysical Journal* **78**, 2761 (2000).
- [13] R. FitzHugh, Impulses and physiological states in theoretical models of nerve membrane, *Biophysical Journal* **1**, 445 (1961).
- [14] J. Nagumo, S. Arimoto, and S. Yoshizawa, An active pulse transmission line simulating nerve axon, *Proceedings of the IRE* **50**, 2061 (1962).
- [15] R. R. Aliev and A. V. Panfilov, A simple two-variable model of cardiac excitation, *Chaos, Solitons & Fractals* **7**, 293 (1996).
- [16] J. Sohl-Dickstein, E. A. Weiss, N. Maheswaranathan, and S. Ganguli, Deep unsupervised learning using nonequilibrium thermodynamics, *CoRR abs/1503.03585* (2015), 1503.03585.
- [17] Y. Song and S. Ermon, Generative modeling by estimating gradients of the data distribution, *CoRR abs/1907.05600* (2019), 1907.05600.
- [18] J. Ho, A. Jain, and P. Abbeel, Denoising diffusion probabilistic models (2020), arXiv:2006.11239 [cs.LG].
- [19] R. Rombach, A. Blattmann, D. Lorenz, P. Esser, and B. Ommer, High-resolution image synthesis with latent diffusion models, *CoRR abs/2112.10752* (2021), 2112.10752.
- [20] C. Saharia, W. Chan, H. Chang, C. A. Lee, J. Ho, T. Salimans, D. J. Fleet, and M. Norouzi, Palette: Image-to-image diffusion models, *CoRR abs/2111.05826* (2021), 2111.05826.
- [21] C. Saharia, W. Chan, S. Saxena, L. Li, J. Whang, E. Denton, S. K. S. Ghasemipour, B. K. Ayan, S. S. Mahdavi, R. G. Lopes, T. Salimans, J. Ho, D. J. Fleet, and M. Norouzi, Photorealistic text-to-image diffusion models with deep language understanding (2022), arXiv:2205.11487 [cs.CV].
- [22] U. Singer, A. Polyak, T. Hayes, X. Yin, J. An, S. Zhang, Q. Hu, H. Yang, O. Ashual, O. Gafni, D. Parikh, S. Gupta, and Y. Taigman, Make-a-video: Text-to-video generation without text-video data (2022), arXiv:2209.14792 [cs.CV].
- [23] Z. Kong, W. Ping, J. Huang, K. Zhao, and B. Catanzaro, Diffwave: A versatile diffusion model for audio synthesis (2021), arXiv:2009.09761 [eess.AS].
- [24] W. H. L. Pinaya, P.-D. Tudosiu, J. Dafflon, P. F. da Costa, V. Fernandez, P. Nachev, S. Ourselin, and M. J. Cardoso, Brain imaging generation with latent diffusion models (2022), arXiv:2209.07162 [eess.IV].
- [25] J. L. Watson, D. Juergens, N. R. Bennett, B. L. Trippe, J. Yim, H. E. Eisenach, W. Ahern, A. J. Borst, R. J. Ragotte, L. F. Milles, B. I. M. Wicky, N. Hanikel, S. J. Pellock, A. Courbet, W. Sheffler, J. Wang, P. Venkatesh, I. Sappington, S. V. Torres, A. Lauko, V. D. Bortoli, E. Mathieu, R. Barzilay, T. S. Jaakkola, F. DiMaio, M. Baek, and D. Baker, Broadly applicable and accurate protein design by integrating structure prediction networks and diffusion generative models, *bioRxiv* 10.1101/2022.12.09.519842 (2022).
- [26] Z. Guo, J. Liu, Y. Wang, M. Chen, D. Wang, D. Xu, and J. Cheng, Diffusion models in bioinformatics and computational biology, *Nature Reviews Bioengineering* 10.1038/s44222-023-00114-9 (2023).
- [27] A. Kazerouni, E. K. Aghdam, M. Heidari, R. Azad, M. Fayyaz, I. Hacihaliloglu, and D. Merhof, Diffusion models in medical imaging: A comprehensive survey, *Medical Image Analysis* **88**, 102846 (2023).
- [28] L. Zhou, Y. Du, and J. Wu, 3d shape generation and completion through point-voxel diffusion, *CoRR abs/2104.03670* (2021), 2104.03670.
- [29] J. Lebert, M. Mittal, and J. Christoph, Reconstruction of three-dimensional scroll waves in excitable media from two-dimensional observations using deep neural networks, *Phys. Rev. E* **107**, 014221 (2023).
- [30] R. Stenger, S. Herzog, I. Kottlarz, B. Rüdhardt, S. Luther, F. Wörgötter, and U. Parlitz, Reconstructing in-depth activity for chaotic 3d spatiotemporal excitable media models based on surface data, *Chaos: An Interdisciplinary Journal of Nonlinear Science* **33**, 013134 (2023), <https://doi.org/10.1063/5.0126824>.
- [31] J. Lebert, D. Deng, L. Fan, L. C. Lee, and J. Christoph, Deep learning-based prediction of electrical arrhythmia

- circuits from cardiac motion: An in-silico study (2023), arXiv:2305.07822 [physics.med-ph].
- [32] C. Zhang, M. Rezavand, Y. Zhu, Y. Yu, D. Wu, W. Zhang, J. Wang, and X. Hu, Sphinxsys: An open-source multi-physics and multi-resolution library based on smoothed particle hydrodynamics, *Computer Physics Communications* **267**, 108066 (2021).
- [33] C. Zhang, J. Wang, M. Rezavand, D. Wu, and X. Hu, An integrative smoothed particle hydrodynamics method for modeling cardiac function, *Computer Methods in Applied Mechanics and Engineering* **381**, 113847 (2021).
- [34] P. Dhariwal and A. Nichol, Diffusion models beat gans on image synthesis, *CoRR* **abs/2105.05233** (2021), 2105.05233.
- [35] L. Jiang and Y. Belousov, Unofficial implementation of Palette: Image-to-image diffusion models, <https://github.com/Janspiry/Palette-Image-to-Image-Diffusion-Models> (2022).
- [36] P. von Platen, S. Patil, A. Lozhkov, P. Cuenca, N. Lambert, K. Rasul, M. Davaadorj, and T. Wolf, Diffusers: State-of-the-art diffusion models.
- [37] O. Ronneberger, P. Fischer, and T. Brox, U-net: Convolutional networks for biomedical image segmentation, in *Lecture Notes in Computer Science* (Springer International Publishing, 2015) pp. 234–241.
- [38] A. Paszke, S. Gross, F. Massa, A. Lerer, J. Bradbury, G. Chanan, T. Killeen, Z. Lin, N. Gimelshein, L. Antiga, A. Desmaison, A. Kopf, E. Yang, Z. DeVito, M. Raison, A. Tejani, S. Chilamkurthy, B. Steiner, L. Fang, J. Bai, and S. Chintala, PyTorch: An Imperative Style, High-Performance Deep Learning Library, in *Advances in Neural Information Processing Systems 32*, edited by H. Wallach, H. Larochelle, A. Beygelzimer, F. d’Alché Buc, E. Fox, and R. Garnett (Curran Associates, Inc., 2019) pp. 8024–8035.
- [39] J. Christoph and J. Lebert, Inverse mechano-electrical reconstruction of cardiac excitation wave patterns from mechanical deformation using deep learning, *Chaos: An Interdisciplinary Journal of Nonlinear Science* **30**, 123134 (2020).
- [40] J. Lebert, N. Ravi, F. H. Fenton, and J. Christoph, Rotor localization and phase mapping of cardiac excitation waves using deep neural networks, *Frontiers in Physiology* **12**, 10.3389/fphys.2021.782176 (2021).
- [41] R. Kazmierczak, G. Franchi, N. Belkhir, A. Manzanera, and D. Filliat, A study of deep perceptual metrics for image quality assessment (2022), arXiv:2202.08692 [cs.CV].
- [42] T. Lilienkamp, J. Christoph, and U. Parlitz, Features of chaotic transients in excitable media governed by spiral and scroll waves, *Phys. Rev. Lett.* **119**, 054101 (2017).
- [43] D. P. Kingma and J. Ba, Adam: A method for stochastic optimization, in *3rd International Conference on Learning Representations, ICLR 2015, San Diego, CA, USA, May 7-9, 2015, Conference Track Proceedings*, edited by Y. Bengio and Y. LeCun (2015).
- [44] M. J. Hoffman, N. S. LaVigne, S. T. Scorse, F. H. Fenton, and E. M. Cherry, Reconstructing three-dimensional reentrant cardiac electrical wave dynamics using data assimilation, *Chaos: An Interdisciplinary Journal of Nonlinear Science* **26**, 013107 (2016).
- [45] M. J. Hoffman and E. M. Cherry, Sensitivity of a data-assimilation system for reconstructing three-dimensional cardiac electrical dynamics, *Philosophical Transactions of the Royal Society A: Mathematical, Physical and Engineering Sciences* **378**, 20190388 (2020).
- [46] K. He, X. Zhang, S. Ren, and J. Sun, Deep residual learning for image recognition, *CoRR* **abs/1512.03385** (2015), 1512.03385.
- [47] Z. Qu, F. Xie, A. Garfinkel, and J. N. Weiss, Origins of spiral wave meander and breakup in a two-dimensional cardiac tissue model, *Annals of Biomedical Engineering* **28**, 755–771 (2000).

VI. SUPPLEMENTARY VIDEOS

The Supplementary Videos can be found at: <https://cardiacvision.ucsf.edu/videos/>.

Supplementary Video 1: Denoising process during reconstruction of a scroll wave pattern inside a bulk-shaped excitable medium. The reconstructions are performed based on observations of the dynamics on the top and bottom surfaces of the bulk, see also Figs. 2 and 3.

Supplementary Video 2: Hallucination of diffusion model during two-dimensional inpainting task for different mask sizes and wave patterns, see Fig. 4.

Supplementary Video 3: Denoising diffusion process for multiple exemplary spiral wave patterns in an unconditional task in which the model can dream up any wave pattern.

Supplementary Video 4: Comparison of spiral wave dynamics evolved with biophysical model (Ground-Truth, left), diffusion (center), and U-Net (right). The diffusion-based solution co-evolves with the solution of the biophysical model. All dynamics start with the same initial wave pattern.

Supplementary Video 5: Comparison of spiral wave dynamics evolved with biophysical model (Ground-Truth, left), diffusion (center), and (absolute) difference between the two patterns. With complicated wave dynamics the solutions of the biophysical model and the diffusion model quickly diverge.

VII. DATA AVAILABILITY STATEMENT

The data that support the findings of this study are available from the corresponding author upon reasonable request.

VIII. FUNDING

This research was funded by the University of California, San Francisco, and the National Institutes of Health (DP2HL168071). The RTX A5000 GPUs used in this

study were donated by the NVIDIA Corporation via the Academic Hardware Grant Program (to JL and JC).

IX. AUTHOR CONTRIBUTIONS

TB developed the deep learning methodology and performed the data analysis. JC aided with the data analysis. JL performed the SPH and bulk simulations. TB and JC designed the figures. JC wrote the manuscript. TB aided in writing the manuscript. All authors discussed

and interpreted the results and read and approved the final version of the manuscript. JL and JC conceived the research.

X. CONFLICT OF INTEREST

The authors declare that the research was conducted in the absence of any commercial or financial relationships that could be construed as a potential conflict of interest.